Arch Toxicol
DOI 10.1007/s00204-017-2066-y

MOLECULAR TOXICOLOGY

t-BuOOH induces ferroptosis in human and murine cell lines

Christine Wenz[1] · Dagmar Faust[1] · Berenike Linz[1] · Christian Turmann[1] · Teodora Nikolova[1] · John Bertin[2] · Peter Gough[2] · Peter Wipf[3] · Anna Sophia Schröder[4] · Stefan Krautwald[4] · Cornelia Dietrich[1]

Received: 15 August 2017 / Accepted: 14 September 2017

Abstract Reactive oxygen species (ROS)-induced apoptosis has been extensively studied. Increasing evidence suggests that ROS, for instance, induced by hydrogen peroxide (H_2O_2), might also trigger regulated necrotic cell death pathways. Almost nothing is known about the cell death pathways triggered by *tertiary*-butyl hydroperoxide (*t*-BuOOH), a widely used inducer of oxidative stress. The lipid peroxidation products induced by *t*-BuOOH are involved in the pathophysiology of many diseases, such as cancer, cardiovascular diseases, or diabetes. In this study, we exposed murine fibroblasts (NIH3T3) or human keratinocytes (HaCaT) to *t*-BuOOH (50 or 200 µM, respectively) which induced a rapid necrotic cell death. Well-established regulators of cell death, i.e., p53, poly(ADP)ribose polymerase-1 (PARP-1), the stress kinases p38 and c-Jun N-terminal-kinases 1/2 (JNK1/2), or receptor-interacting serine/threonine protein kinase 1 (RIPK1) and 3 (RIPK3), were not required for *t*-BuOOH-mediated cell death. Using the selective inhibitors ferrostatin-1 (1 µM) and liproxstatin-1 (1 µM), we identified ferroptosis, a recently discovered cell death mechanism dependent on iron and lipid peroxidation, as the main cell death pathway. Accordingly, *t*-BuOOH exposure resulted in a ferrostatin-1- and liproxstatin-1-sensitive increase in lipid peroxidation and cytosolic ROS. Ferroptosis was executed independently from other *t*-BuOOH-mediated cellular damages, i.e., loss of mitochondrial membrane potential, DNA double-strand breaks, or replication block. H_2O_2 did not cause ferroptosis at equitoxic concentrations (300 µM) and induced a (1) lower and (2) ferrostatin-1- or liproxstatin-1-insensitive increase in lipid peroxidation. We identify that *t*-BuOOH and H_2O_2 produce a different pattern of lipid peroxidation, thereby leading to different cell death pathways and present *t*-BuOOH as a novel inducer of ferroptosis.

Keywords Oxidative stress · *t*-BuOOH · Ferroptosis · Lipid peroxidation

Introduction

Oxidative stress results from an imbalance of oxidative versus anti-oxidative processes and species. Overproduction of reactive oxygen species (ROS) plays a fundamental role in the pathogenesis of neurodegenerative diseases, inflammation, cardiovascular disorders (e.g., ischemia), diabetes, and cancer (Sedelnikova et al. 2010; Sosa et al. 2013). ROS might derive from endogenous sources, i.e., ROS-generating enzymes or mitochondrial leakage, or from exogenous sources, such as irradiation, UV light, xenobiotic metabolization, or others (Sosa et al. 2013). Detrimental ROS include peroxides (H_2O_2 and ROOH), the superoxide radical anion ($O_2^{\cdot -}$), and neutral radicals ($RO^{\cdot}$ and $OH^{\cdot}$) which induce a plethora of cellular damages, e.g., collapse of mitochondrial

Electronic supplementary material The online version of this article (doi:10.1007/s00204-017-2066-y) contains supplementary material, which is available to authorized users.

✉ Cornelia Dietrich
cdietric@uni-mainz.de

[1] Institute of Toxicology, University Medical Center of the Johannes Gutenberg-University, Obere Zahlbacherstr. 67, 55131 Mainz, Germany

[2] Pattern Recognition Receptor Discovery Performance Unit, Immuno-Inflammation Therapeutic Area, GlaxoSmithKline, Collegeville, PA 19426, USA

[3] Department of Chemistry, University of Pittsburgh, 219 Parkman Avenue, Pittsburgh, PA 15260, USA

[4] Department of Nephrology and Hypertension, University Hospital Schleswig-Holstein, 24105 Kiel, Germany

Published online: 03 October 2017

membrane potential (MMP), DNA single- and double-strand breaks (SSBs and DSBs), replication block as well as DNA base, lipid, and protein oxidation (Avery 2011; Wang 2008). Excess cellular damage finally leads to cell death. ROS-induced apoptosis has been extensively studied including the interplay between DNA damage and mitochondrial function (Redza-Dutordoir and Averill-Bates 2016).

Apoptosis has long been considered to be the sole pathway of regulated cell death. In contrast, necrosis was generally regarded as accidental. Increasing evidence demonstrates that necrosis may also be executed by defined cellular programs. According to their regulated nature, these pathways are classified as "regulated necrosis" (Galluzzi et al. 2012, 2014; Linkermann et al. 2014b). One of the best studied regulated necrotic pathways is necroptosis. Among others, necroptosis can be initiated by TNFα receptor activation and is mediated by RIPK3, which generally, but not necessarily, interacts with RIPK1 (Conrad et al. 2016; Linkermann and Green 2014; Vanden Berghe et al. 2014). RIPK3 ultimately activates the executioner mixed lineage kinase domain-like pseudokinase (MLKL). Severe DNA damage may lead to hyperactivation of poly(ADP) ribose polymerase-1 (PARP-1) and subsequent depletion of NAD^+, a process called parthanatos (Andrabi et al. 2008; Wang et al. 2009). Another form of regulated necrosis is mitochondrial permeability transition (MPT)-mediated necrosis due to opening of the MPT pore complex, which is dependent on cyclophilin D (Baines et al. 2005; Halestrap 2009; Linkermann et al. 2013). Ferroptosis is a recently discovered necrotic pathway characterized by iron dependence and lipid peroxidation induced, for instance, by erastin, or inhibition of the glutathione peroxidase 4 (GPX4) (Cao and Dixon 2016; Dixon 2017; Dixon et al. 2012; Friedmann Angeli et al. 2014; Linkermann et al. 2014a; Xie et al. 2016; Yang et al. 2014; Yang and Stockwell 2016). Although the precise molecular mechanisms of these newly identified necrotic pathways remain to be clarified, the importance of regulated necrosis during embryonic development and under pathophysiological conditions is widely accepted. Regulated necrosis is not only involved in pathological processes, such as ischemia reperfusion injury in kidney, heart, brain and liver, inflammatory bowel disease, atherosclerosis, neuronal degeneration, and others (Tonnus and Linkermann 2017), but it is also important to overcome apoptosis resistance in tumor cells (Fulda 2014; Kreuzaler and Watson 2012; Mohammad et al. 2015).

Regulated necrosis can be triggered by a variety of stimuli, such as receptors, pathogens, or genotoxic stress (Vanden Berghe et al. 2014; Vanlangenakker et al. 2012). Increasing evidence suggests that regulated necrosis may also be induced by ROS. Here, especially, the role of H_2O_2 (hydrogen peroxide) has been investigated. H_2O_2 can cause parthanatos (Xu et al. 2013) or MPT-mediated necrosis (Baines et al. 2005). Activation of RIPK1 by H_2O_2 has also been described (Shen et al. 2004).

Among the substances to induce ROS experimentally, H_2O_2 and the organic peroxide *tertiary*-butyl hydroperoxide (*t*-BuOOH) are the most frequently used compounds. In general, no discrimination is made between the use of these reagents and a similar mechanism of action is assumed. Both are known to produce radicals leading to DNA damage, loss of MMP, and oxidation of proteins and lipids. However, several observations led us to hypothesize that the compounds might differ in their mode of action: (1) *t*-BuOOH shows a higher intracellular stability than H_2O_2 thus leading to a persistent oxidative stress in contrast to H_2O_2 (Alia et al. 2005; Baker and He 1991); (2) H_2O_2 freely penetrates the cell, thereby targeting a variety of cellular structures. Local production of the hydroxyl radical via the Fenton reaction, e.g., at the sites of DNA, is known to finally induce cellular damage (Bergamini et al. 2004). In contrast, the organic peroxide *t*-BuOOH is more lipophilic than H_2O_2 suggesting a predominant action on cellular membranes as it has been shown for cumene hydroperoxide (Vroegop et al. 1995); (3) in accordance with an action on biological membranes, one hallmark of *t*-BuOOH use is lipid peroxidation (Barr and Mason 1995; Coleman et al. 1989; Masaki et al. 1989). For instance, lipid peroxidation was only induced by the lipophilic *t*-BuOOH or cumene hydroperoxide, but not by H_2O_2, in glioma cells or in a human adenocarcinoma cell line (Baker and He 1991; Linden et al. 2008). Lipid peroxidation products formed by *t*-BuOOH, e.g., malondialdehyde or 4-hydroxynonenal, are pathophysiologically relevant. They are produced and involved in the development of many diseases, such as Alzheimer's disease, Parkinson's disease, cancer, diabetes, or cardiovascular diseases (Ayala et al. 2014; Garcia-Cohen et al. 2000; Lemasters and Nieminen 1997).

Although *t*-BuOOH is frequently used to induce oxidative stress, the mechanism of cell death induced by this reagent is largely unknown. In view of the above-mentioned role of ROS in many diseases and especially the pathophysiological relevance of lipid peroxidation products, we analyzed more deeply the cell death events triggered by *t*-BuOOH. Murine NIH3T3 fibroblasts were chosen as the main cellular system as they are able to undergo not only apoptosis, but also regulated necrosis, such as necroptosis, parthanatos, MPT-driven necrosis, or ferroptosis (Baines et al. 2005; Chiu et al. 2011; Friedmann Angeli et al. 2014; Shen et al. 2004; Zhang et al. 2011). Results were verified in a human keratinocyte cell line (HaCaT) to rule out cell type-specific effects. Here, we show that *t*-BuOOH induces regulated necrosis in vitro and we identified ferroptosis as the main cell death pathway. Although *t*-BuOOH induces a plethora of cellular detriments, i.e., dissipation of the MMP, DNA DSBs, and replication block, *t*-BuOOH-mediated ferroptosis is executed independently from these damages. Importantly,

H_2O_2 does not induce ferroptosis at an equitoxic concentration. This observation strongly indicates that the mode of action of *t*-BuOOH and H_2O_2 is indeed dissimilar. We conclude that individual ROS inducers may trigger different cell death pathways which might depend on the nature of the ROS species formed, its amount or kinetics, and/or subcellular localization. In contrast to other chemical ROS inducers tested so far, *t*-BuOOH can trigger a ferroptotic cell death mechanism.

Materials and methods

Chemicals

t-BuOOH, H_2O_2, staurosporine, ferrostatin-1, liproxstatin-1, α-tocopherol, and *N*-acetylcysteine were purchased from Sigma-Aldrich (St. Louis, MO, USA), z-VAD-fmk from Promega (Madison, WI, USA), and cisplatin from the Pharmacy of the University Medical Center (Mainz, Germany). Olaparib was obtained from Selleckchem (Houston, TX, USA), necrostatin-1 from Santa Cruz Biotechnology (CA, USA), and deferoxamine mesylate from Tocris (Avonmouth, Bristol, UK). The RIPK1 inhibitors GSK2791728A, GSK3002963A, the RIPK3 inhibitors GSK2393843A, and GSK2399872B were provided by Peter Gough (GlaxoSmithKline, Collegeville, PA, USA). XJB-5-131 and JP-4-039 were synthesized by Peter Wipf (University of Pittsburgh, PA, USA).

Cell culture

Non-transformed murine fibroblasts (NIH3T3) (Dietrich et al. 1997), $p53^{+/+}$ (wt) and $p53^{-/-}$ mouse embryonic fibroblasts (Lackinger et al. 2001) (kind gift by Markus Christmann, Mainz, Germany), and human keratinocytes (HaCaT) (Boukamp et al. 1988) (kind gift by Norbert Fusenig, German Cancer Research Center, Heidelberg, Germany) were routinely cultured in Dulbecco's Modified Eagle's Medium (DMEM, Gibco Life Technologies, Carlsbad, CA, USA), supplemented with 2 mM glutamine, penicillin, and streptomycin (each 100 U/mL), and 10% fetal bovine serum (FBS). Cells were kept at 37 °C in a humidified atmosphere containing 5% CO_2. For the experiments, NIH3T3 and HaCaT cells were sparsely seeded (8×10^3 cells/cm^2), cultured for 24 h and then treated with *t*-BuOOH at a concentration of 50 µM (NIH3T3) or 200 µM (HaCaT), respectively, except where otherwise specified.

Determination of cell viability (Trypan blue exclusion)

For determination of viability, cells were washed, trypsinized, incubated with Trypan blue, and counted in a hemocytometer. The viability was checked by Trypan blue exclusion.

Determination of cell death

Cells were washed, trypsinized, and pelletized together with the supernatant by centrifugation. After repeated washing, the cell pellet was resuspended in 250 µL of 1× Annexin-binding buffer (10×: 100 mM HEPES, 1.4 M NaCl, 25 mM $CaCl_2$, 1% BSA ad 50 mL purified water; pH 7.4; all reagents provided by Carl Roth, Karlsruhe, Germany) containing 5% AnnexinV-FITC (Miltenyi Biotec, Bergisch Gladbach, Germany), incubated for 15–20 min, followed by dropwise addition of 1 mg/mL propidium iodide (PI, Applichem, Darmstadt, Germany). 10,000 cells per sample were scored and the ratio between apoptosis and necrosis was determined by BD CellQuest Pro (FACS Calibur) or BD FACS Diva software (FACS CantoII).

Western blot analysis

Cells were lysed in hot Laemmli sample buffer (Laemmli 1970). Protein concentration was determined according to (Smith et al. 1985). Equal amounts of protein (50 µg per lane) were separated by SDS-PAGE (7.5–12.5%) and electroblotted onto Immobilon membranes (Merck Millipore, Darmstadt, Germany). The blots were either blocked for 1 h with 5% low-fat milk powder in TBS (50 mM Tris–HCl, pH 7.5, 150 mM NaCl) containing 0.05% Tween 20 and then incubated for 1.5 h at room temperature with anti-cleaved caspase 3 antibody (1:1000, Santa Cruz) or anti-p53 antibody (Merck Millipore), or the blots were blocked with 5% bovine serum albumine (BSA) and then incubated overnight at 4 °C with phospho-specific (T71) anti-ATF2 or phospho-specific (T334) anti-MAPKAP antibody (each 1:1000, Cell Signaling, Beverly, MA, USA) followed by incubation with horseradish-peroxidase-conjugated secondary antibody and ECL detection (Cell Signaling) according to the manufacturer's instructions. To control for equal loading, the blots were stripped and reprobed with anti-HSP90 antibody, anti-ATF2 antibody, or anti-MAPKAP antibody (each 1:1000, Santa Cruz) followed by ECL detection.

Immunocytochemistry

For detection of PAR foci, HaCaT cells were seeded on sterile cover slips and were untreated or pre-incubated with olaparib (0.5 µM, 1 h) prior to treatment with 5 mM *t*-BuOOH in phosphate buffered saline (PBS) for 7 min at 37 °C. Subsequently, cells were fixed in methanol (−20 °C, 7 min). Cells were then washed, incubated with 5% milk powder (Carl Roth), diluted in PBS/0.1% Tween 20 (Sigma-Aldrich) for 30 min (RT), followed by application of the

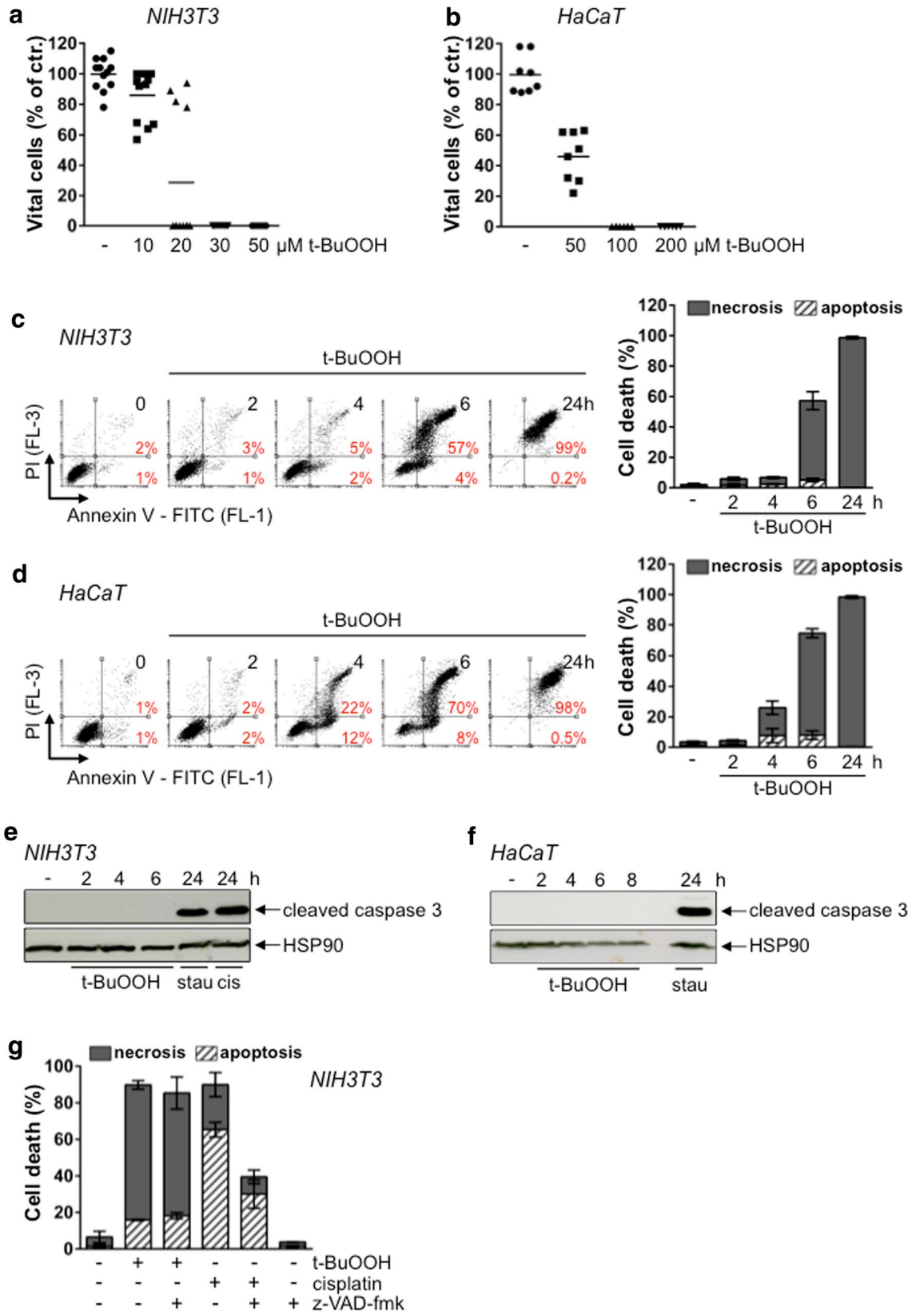
a
NIH3T3
Vital cells (% of ctr.)
120
100
80
60
40
20
0
- 10 20 30 50 µM t-BuOOH
b
HaCaT
Vital cells (% of ctr.)
- 50 100 200 µM t-BuOOH
c
NIH3T3
t-BuOOH
0
2
4
6
24h
2%
1%
3%
1%
5%
2%
57%
4%
99%
0.2%
PI (FL-3)
Annexin V - FITC (FL-1)
necrosis
apoptosis
Cell death (%)
- 2 4 6 24 h
t-BuOOH
d
HaCaT
t-BuOOH
0
2
4
6
24h
1%
1%
2%
2%
22%
12%
70%
8%
98%
0.5%
PI (FL-3)
Annexin V - FITC (FL-1)
necrosis
apoptosis
Cell death (%)
- 2 4 6 24 h
t-BuOOH
e
NIH3T3
- 2 4 6 24 24 h
cleaved caspase 3
HSP90
t-BuOOH
stau
cis
f
HaCaT
- 2 4 6 8 24 h
cleaved caspase 3
HSP90
t-BuOOH
stau
g
necrosis
apoptosis
NIH3T3
Cell death (%)
100
80
60
40
20
0
- + + - - - t-BuOOH
- - - + + - cisplatin
- - + - + + z-VAD-fmk

◂**Fig. 1** *t*-BuOOH induces necrosis in NIH3T3 and HaCaT cells. **a, b** Cell viability after *t*-BuOOH treatment assessed by Trypan blue exclusion assay. NIH3T3 (**a**) or HaCaT (**b**) cells were treated with *t*-BuOOH for 24 h at the indicated concentrations. Results are given in % of untreated controls. **c, d** Cell death in response to *t*-BuOOH determined by Annexin V-FITC/PI staining. NIH3T3 (**c**) or HaCaT (**d**) cells were treated with 50 or 200 µM *t*-BuOOH, respectively, and cell death was measured at the indicated timepoints. Annexin V^+/PI^+ cells represent the late apoptotic/necrotic fraction, Annexin V^+/PI^- cells in general the early apoptotic fraction. However, we cannot rule out that the Annexin V^+/PI^- cells represent a population undergoing early regulated necrosis (Gong et al. 2017). (Left) Representative dot plots. (Right) mean ± SD, $n = 3$ in duplicates. Induction of necrosis was highly significant ($p < 0.001$) from 6 h on. **e, f** Western blot analysis. NIH3T3 (**e**) or HaCaT (**f**) cells were treated with *t*-BuOOH (50 or 200 µM, respectively), staurosporine (stau, 1 µM) or cisplatin (cis, 40 µM) and harvested at the indicated timepoints. Western blot analysis was performed using anti-cleaved caspase 3 antibody. Blots were stripped and reprobed with anti-HSP90 antibody to control equal loading. **g** Determination of cell death. NIH3T3 cells were pretreated with z-VAD-fmk (20 µM) and then exposed to *t*-BuOOH (50 µM) or cisplatin (40 µM) for 24 h. Z-VAD-fmk significantly ($p < 0.001$) inhibited cisplatin-induced cell death, but did not block *t*-BuOOH-mediated cell death. Results are expressed as mean ± SD, $n = 3$ in duplicates

primary antibody for PAR foci detection (anti-10H antibody, 1:300, 1 h, RT, and kindly provided by Alexander Bürkle, Konstanz, Germany). After washing, cells were incubated for 1 h with Alexa Fluor 488-labeled secondary antibody at RT (1:400, Gibco Life Technologies) and nuclei were counterstained with To-Pro-3 (1:100 in PBS, Thermofisher Scientific, Waltham, MA, USA). After washing, antifade medium (Vectashield, Vector Laboratories, CA, USA) was dropped onto clean slides and the cover slips were transferred onto the slides and fixed with nail polish.

Replication block was demonstrated by the reduction of EdU-positive S-phase cells. EdU staining was performed using the Click-iT EdU Alexa Fluor 555 Imaging Kit (Thermofisher Scientific) according to the manufacturer's instructions. Nuclei were counterstained for 15 min with To-Pro-3 (1:100 in PBS). After washing, antifade medium was dropped onto clean slides and the cover slips were transferred onto the slides and fixed with nail polish. The mean fluorescence intensity of the fluorescent dye (Alexa Fluor 555) bound to EdU was measured for each cell captured onto LSM710 images using "BIC Macro Toolkit" (https://www.bioimaging-center.uni-konstanz.de/image-analysis/bic-macro-toolkit/). Representative confocal images were captured by the ZEN2009 software for laser scanning microscopy (LSM710; Zeiss, Oberkochen, Germany).

Generating stable CRISPR/Cas9 knockout NIH3T3 cells

The sgRNAs for the selected targets RIPK1 and RIPK3 were designed in silico via the CRISPR Design Tool (http://tools.genome-engineering.org). The single-stranded sgRNA oligos were annealed and ligated into an expression plasmid bearing both sgRNA scaffold backbone and Cas9 (pX330-U6-Chimeric_BB-CBh-hSpCas9, Addgene plasmid no. 42230) as previously described in detail (Muller et al. 2017). The resulting plasmids (annotated as pSpCas9_sgRNA) were then co-transfected with the pcDNA3.1(+) vector (Invitrogen, no. V790-20) containing a geneticin resistance gene into target cells. After single-cell cloning by serial dilution in 96-well plates (media were supplemented with 1 mg/mL G418), the clones were assayed and selected for their target gene-knockout by Western blot analysis to identify stable CRISPR/Cas9-ko cell lines.

Detection of cytosolic and lipid ROS

The cytosolic ROS assay was conducted as previously described (Faust et al. 2017). Cells were washed with PBS, covered with MEM without phenol red and incubated with the ROS probe 2-7-dichlorodihydrofluorescein diacetate (H_2DCFDA; Sigma-Aldrich) for 30 min at 37 °C. Cells were washed with PBS, covered with MEM without phenol red, and treated with *t*-BuOOH (50 µM) for 2 h. Cells were then washed with PBS, trypsinized, and pelletized by centrifugation. Cells were resuspended in PBS and flow cytometric analysis was performed by a FACS CantoII (BD Becton Dickinson, Heidelberg, Germany). Detection of lipid ROS was performed accordingly using the lipid ROS probe Bodipy 581/591 C11 (Life Technologies).

Detection of mitochondrial membrane potential ($\psi\Delta_m$)

Loss of $\psi\Delta_m$ was detected by staining with DiOC6 (3,3′-dihexyloxacarbocyanine iodide) (Thermofisher Scientific). The supernatant including dead cells was collected and stored on ice. Adherent cells were washed and stained with 20 nM DiOC6 for 20 min at 37 °C. After trypsinization, cells were pelletized together with the supernatant by centrifugation, followed by dropwise addition of propidium iodide to detect necrotic cells as described above. Analysis was performed by flow cytometry (FACS CantoII).

Neutral comet assay

The cells were harvested and subjected to a neutral Comet assay. About 10^4 cells were mixed with 120 µL low melting agarose (0.5%) and transferred onto slides precoated with agarose. Lysis (2.5 M NaCl, 100 mM EDTA, 10 mM Tris, pH 7.5) was performed for 50 min at 4 °C. Cells were placed in an electrophoresis chamber and mounted in a neutral electrophoresis buffer (90 mM Tris, 2 mM EDTA, 90 mM boric

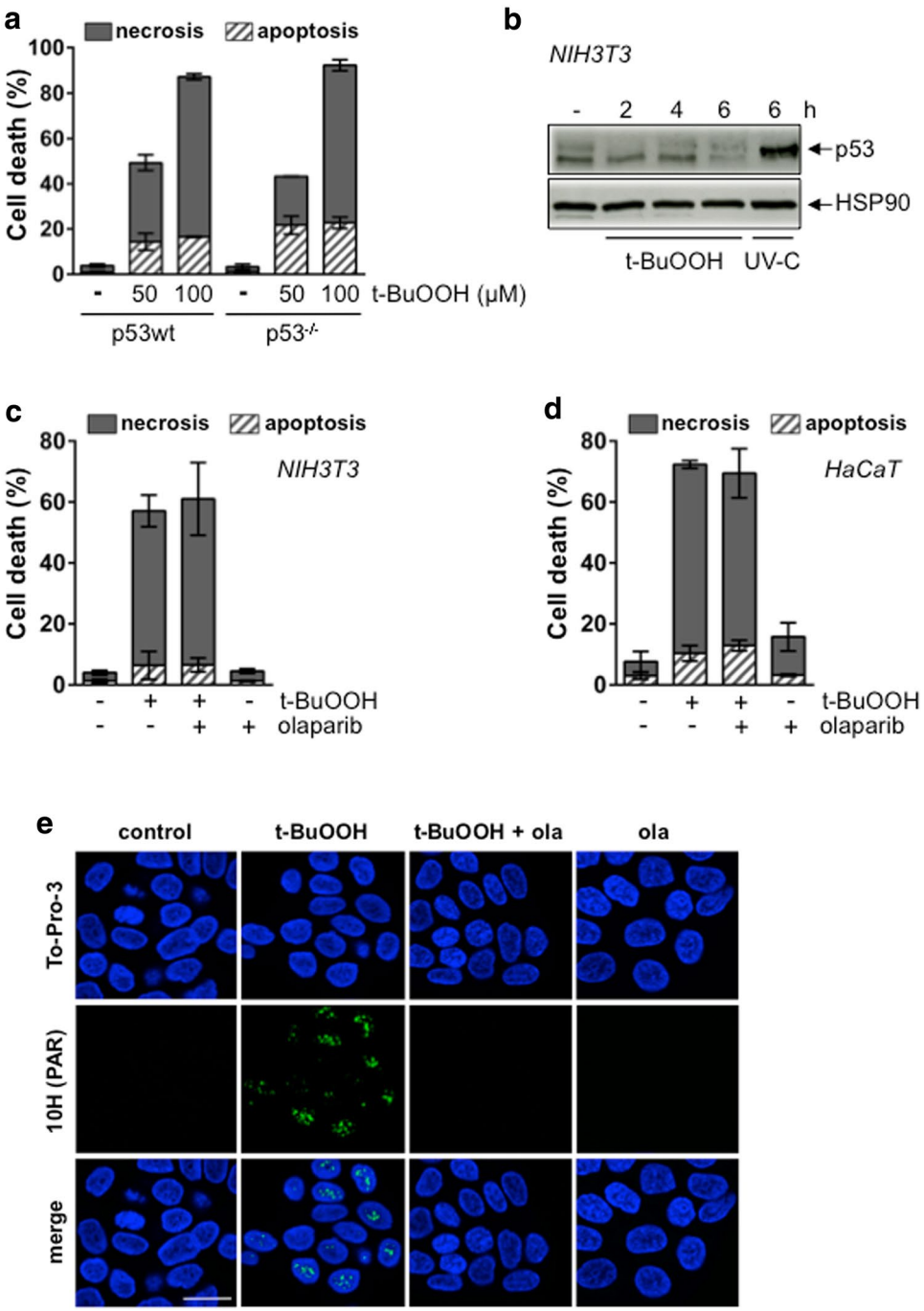

Fig. 2 p53 and PARP-1 are not involved in *t*-BuOOH-triggered cell death. **a** Determination of cell death. p53wt and $p53^{-/-}$ MEFs were treated with *t*-BuOOH for 24 h at the indicated concentrations. Results are expressed as mean ± SD, $n = 2$ in duplicates. *t*-BuOOH significantly ($p < 0.001$) induced cell death in p53wt and $p53^{-/-}$ MEFs. **b** Western blot analysis. NIH3T3 cells were treated with *t*-BuOOH or UV-C (20 J/m^2) and harvested at the indicated timepoints. Western blot analysis was performed using anti-p53 antibody. Blots were stripped and reprobed with anti-HSP90 antibody to control equal loading. **c**, **d** Determination of cell death. NIH3T3 (**c**) or HaCaT (**d**) cells were pretreated with olaparib (0.5 µM) and then treated with *t*-BuOOH (30 or 200 µM, respectively) for 6 h. Results are expressed as mean ± SD, $n = 3$ in duplicates. **e** Determination of protein PARylation. HaCaT cells were pretreated with olaparib (ola, 0.5 µM) and then treated with *t*-BuOOH (5 mM) for 7 min. PAR foci were detected by incubation with anti-PAR antibody followed by Alexa Fluor 488-labeled secondary antibody. Nuclei were counterstained with To-Pro-3. Representative confocal images were captured. Bar = 20 µm

acid, and pH 7.4). After electrophoresis (25 V and 300 mA for 20 min), slides were washed with purified water, air-dried for 2 h with 100% ethanol (Carl Roth), and then stained with 50 µg/mL propidium iodide. Comets were analyzed by fluorescence microscopy using an Olympus BX50 equipped with a ColorView camera (Olympus, Münster, Germany). At least 50 cells/slide were scored using the Comet IV software (Perceptive Instruments Ltd., Bury St Edmunds, UK).

Statistical analyses

Although the results were obvious, comparisons between treatments were made by one- or two-way analysis of variance (ANOVA) followed by Tuckey's multiple comparisons test. A p value of less than 0.05 was considered to be significant.

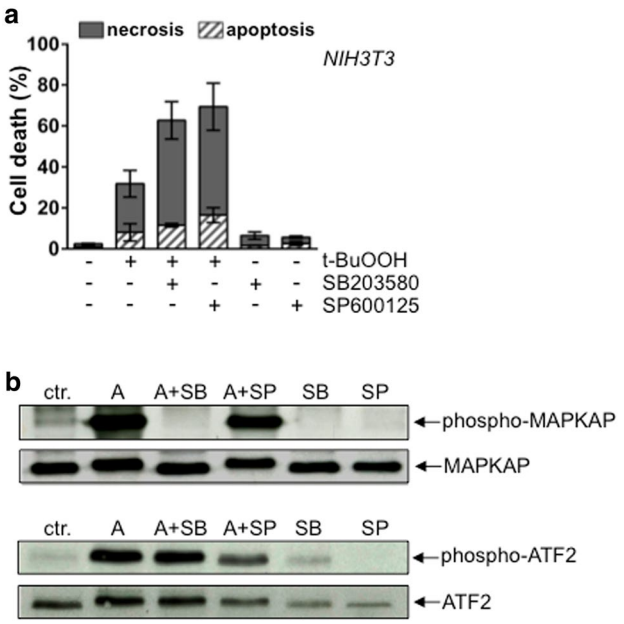

Fig. 3 Stress kinases p38 and JNK1/2 are not involved in *t*-BuOOH-triggered cell death. **a** Determination of cell death. NIH3T3 cells were treated with *t*-BuOOH for 6 h in the absence or the presence of the p38 inhibitor SB203580 (10 µM) or the JNK1/2 inhibitor SP600125 (25 µM). Results are expressed as mean ± SD, $n = 2–5$ in duplicates. **b** Western blot analysis. NIH3T3 cells were treated with anisomycin (A) for 15 min in the absence or the presence of SB203580 or SP600125. Western blot analysis was performed using phospho-specific (T71) anti-ATF2 or phospho-specific (T334) anti-MAPKAP antibody. Blots were stripped and reprobed with anti-ATF-2 or anti-MAPKAP antibody to control equal loading

Results and discussion

t-BuOOH induces necrosis in NIH3T3 and HaCaT cells

NIH3T3 or HaCaT cells were treated for 24 h with indicated concentrations of *t*-BuOOH. Entire cell death was obtained in NIH3T3 cells at a concentration of > 30 µM (Fig. 1a), in HaCaT cells at a concentration of > 100 µM (Fig. 1b). In NIH3T3 cells, the concentration-response relationship indicates a toxic threshold concentration around 20 µM. Annexin V-FITC/PI staining and subsequent flow cytometry revealed that NIH3T3 and HaCaT cells died by necrosis, whereas apoptosis could either not be detected or was marginal at any timepoint (Fig. 1c, d, Supplementary Fig. S1). To confirm our observation, we analyzed cleavage of caspase 3, an important executioner caspase mediating apoptosis. Cleavage of caspase 3 was only observed after treatment with cisplatin or staurosporine, but not in response to *t*-BuOOH (Fig. 1e, f). In agreement with these observations, the pan-caspase inhibitor z-VAD-fmk did not inhibit *t*-BuOOH-induced cell death, but did so in control experiments using cisplatin (Fig. 1g). These data demonstrate that both cell lines are sensitive for apoptotic stimuli. We conclude that *t*-BuOOH triggers necrosis, but not apoptosis, in NIH3T3 and in HaCaT cells in our experimental setup. It has been shown before that low concentrations of H_2O_2 induce apoptosis, whereas higher concentrations of H_2O_2 lead to necrosis, possibly due to ATP depletion (Hampton and Orrenius 1997; Leist et al. 1997; Nicotera and Melino 2004; Saito et al. 2006). However, treatment of NIH3T3 cells with low concentrations of *t*-BuOOH (10 µM) for 48 or 72 h did not induce cell death (unpublished observation). To the best of our knowledge, only few data have been reported on apoptosis in response to *t*-BuOOH, i.e., in human neuroblastoma, hepatoma cells, and human macrophages (Amoroso et al. 2002; Friedemann et al. 2014; Kanupriya et al. 2007; Martin et al. 2010). Hence, induction of apoptosis in response to *t*-BuOOH might either be dependent on the concentration and/or the cell line used.

p53 is not involved in *t*-BuOOH-induced cell death

To elucidate the molecular mechanism of *t*-BuOOH-induced cell death, we investigated the role of potential mediators and focused our interest on p53. Beside its well-established role in regulating apoptosis, p53 has been shown to regulate H_2O_2-induced regulated necrosis, i.e., MPT-driven (Vaseva et al. 2012) and PARP-dependent necrosis (Montero et al. 2013). In mouse embryonic fibroblasts which were derived from $p53^{-/-}$ mice (Lackinger et al. 2001) (Supplementary Fig. S2), *t*-BuOOH induced a similar toxicity after 24 h compared to wt-fibroblasts (Fig. 2a) arguing against a role of p53 in *t*-BuOOH-driven cell death. We could not detect accumulation of p53 protein in response to *t*-BuOOH in NIH3T3 cells, while in control experiments, UV-C treatment caused significant upregulation of p53 protein (Fig. 2b). However, a slight increase in Ser15-phosphorylation was observed (Supplementary Fig. S3), indicating that *t*-BuOOH induced DNA damage (see below). Together with the fact that HaCaT cells exhibit mutated p53 (Lehman et al. 1993), we conclude that p53 is not essential for *t*-BuOOH-induced necrosis. These data further support our hypothesis that H_2O_2- and *t*-BuOOH-mediated necrosis is mediated by different pathways.

PARP-1 activation is not involved in *t*-BuOOH-induced cell death

Severe DNA damage mediated by H_2O_2 may lead to activation of PARP-1, subsequent NAD^+ and ATP depletion, release of apoptosis-inducing factor (AIF) from the mitochondria, translocation of AIF to the nucleus, and finally large-scale DNA fragmentation. This kind of cell death is referred to as parthanatos (Ha and Snyder 1999; Montero et al. 2013; Xu et al. 2013). We, therefore, analyzed a

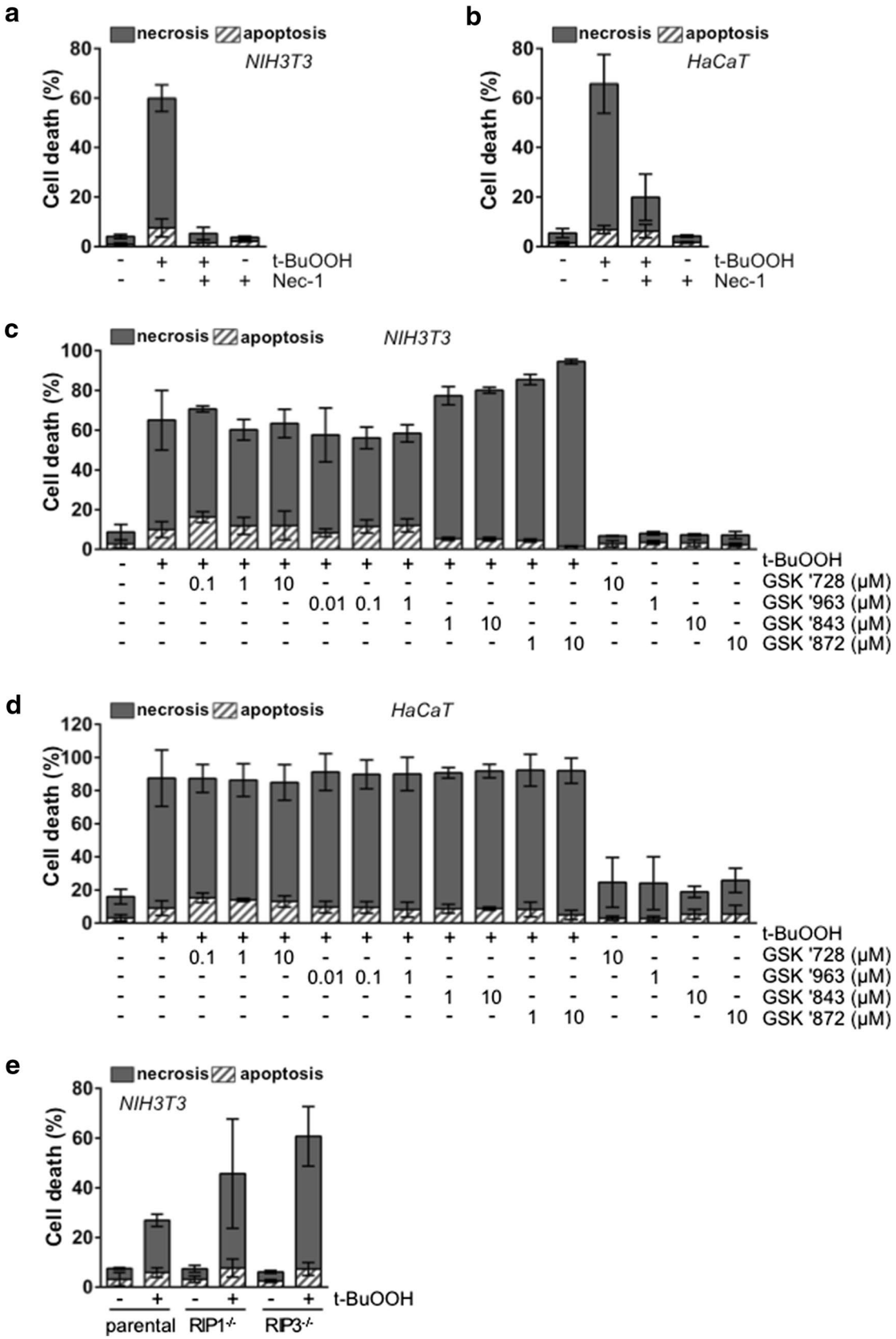
a
necrosis
apoptosis
NIH3T3
Cell death (%)
t-BuOOH
Nec-1
b
HaCaT
c
GSK '728 (μM)
GSK '963 (μM)
GSK '843 (μM)
GSK '872 (μM)
d
e
parental
RIP1-/-
RIP3-/-

◂**Fig. 4** RIPK1 and RIPK3 are not involved in *t*-BuOOH-triggered cell death. **a–e** Determination of cell death. **a–d** NIH3T3 cells (**a**, **c**) or HaCaT cells (**b**, **d**) were exposed to *t*-BuOOH for 6 h in the absence or the presence of necrostatin-1 (Nec-1, 50 μM) (**a**, **b**), the RIPK1 inhibitors GSK'728 or GSK'936, or the RIPK3 inhibitors GSK'843 or GSK'872 (**c**, **d**). Results are expressed as mean ± SD, $n = 2–5$ in duplicates. Nec-1 significantly ($p < 0.001$) inhibited *t*-BuOOH-induced cell death in NIH3T3 and HaCaT cells. **e** Parental, $RIP1^{-/-}$ and $RIP3^{-/-}$ NIH3T3 cells were treated with *t*-BuOOH (50 μM) for 6 h. Results are expressed as mean ± SD, $n = 3$ in duplicates

potential role of PARP-1 in *t*-BuOOH-triggered cell death. Pharmacological inhibition of PARP-1 by olaparib (Menear et al. 2008) did not block *t*-BuOOH-mediated necrosis, neither in NIH3T3 cells (Fig. 2c) nor in HaCaT cells (Fig. 2d). Importantly, olaparib totally abolished PARylation of proteins in HaCaT cells which could be induced by high concentrations of *t*-BuOOH (Fig. 2e) or H_2O_2 (Supplementary Fig. S4) as assessed by immunofluorescence studies using an anti-PAR antibody. These data argue against a potential role of PARP-1 in *t*-BuOOH-induced necrosis and parthanatos as the relevant pathway of cell death.

The stress kinases JNK1/2 and p38 are not required for *t*-BuOOH-induced cell death

The stress kinases JNK1/2 and p38 have both been described to be involved in apoptotic and non-apoptotic cell death induced by H_2O_2 (Gaballah et al. 2012; Kim et al. 2009; Shen et al. 2004; Watanabe et al. 2015; Xia et al. 2009; Zhang et al. 2007). However, also protective, anti-apoptotic functions of p38 and JNK1/2 are known (Deng et al. 2001; Pereira et al. 2013; Sabapathy et al. 1999). Pharmacological inhibition of p38 by SB203580 (Cuenda et al. 1995) or JNK1/2 by SP600125 (Bennett et al. 2001) did not prevent, but augmented *t*-BuOOH-triggered cell death (Fig. 3a). In control experiments, both inhibitors blocked phosphorylation of the p38 and JNK1/2 downstream targets MAPKAP and ATF-2, respectively (Fig. 3b). Our data indicate that, very likely, p38 and JNK1/2 are activated in response to *t*-BuOOH, but that p38 and JNK1/2 have rather protective functions. Our data suggest for the first time that p38 and JNK1/2 might not only protect against apoptosis, but also against necrosis.

RIPK1 and RIPK3 are not involved in *t*-BuOOH-induced cell death

After having ruled out p53, PARP-1 and stress kinases as relevant mediators of *t*-BuOOH-induced cell death, we investigated a potential involvement of RIPK1 or RIPK3 in *t*-BuOOH-triggered necrosis. Although the data are controversial (Degterev et al. 2005; Vanden Berghe et al. 2010; Wang et al. 2012), some authors have described a functional role of RIPK1 in H_2O_2-induced cell death (Shen et al. 2004; Temkin et al. 2006). Cell death was almost completely blocked after 6 h in the presence of necrostatin-1 (Nec-1), a widely used RIPK1 inhibitor (Degterev et al. 2005), in NIH3T3 and HaCaT cells (Fig. 4a, b). To confirm the role of RIPK1 in *t*-BuOOH-mediated necrosis, we made use of the more selective RIPK1 inhibitors GSK'728 and GSK'963 (Berger et al. 2015). To our surprise, *t*-BuOOH-induced cell death could not be blocked by these compounds (Fig. 4c, d). Furthermore, the RIPK3-selective inhibitors GSK'843 and GSK'872 (Dondelinger et al. 2014; Mandal et al. 2014) did not attenuate *t*-BuOOH-mediated cell death in NIH3T3 or HaCaT cells (Fig. 4c, d). Importantly, GSK'728, GSK'936, GSK'843, and GSK'872 significantly reduced necroptosis induced by treatment of mouse embryonic fibroblasts (MEFs) with TNFα/z-VAD-fmk/cycloheximide (Supplementary Fig. S5). Finally, to prove that neither RIPK1 nor RIPK3 is required for *t*-BuOOH-induced cell death, we analyzed NIH3T3 cells after having knocked out RIPK1 or RIPK3 using the CRISPR (clustered regularly interspaced short palindromic repeat)/Cas9 technique. Figure 4e demonstrates that neither deficiency in RIPK1, nor in RIPK3 led to reduction of *t*-BuOOH-induced cell death, but rather sensitized the cells to undergo necrosis. A similar sensitization towards ferroptosis by inhibiting mediators of necroptosis has been described very recently (Muller et al. 2017). Therefore, we conclude that RIPK1 and RIPK3 are not required for *t*-BuOOH-mediated cell death and that Nec-1 exerts an off-target effect in our system (Eling et al. 2015; Friedmann Angeli et al. 2014; Vandenabeele et al. 2013).

t-BuOOH induces ferroptosis

Although still controversial (Dixon et al. 2012), some evidence suggests that Nec-1 blocks ferroptosis, at least at higher concentrations (Eling et al. 2015; Friedmann Angeli et al. 2014). Ferroptosis is a newly discovered iron-dependent cell death pathway characterized by lipid peroxidation, but independent from caspases and RIPK1/RIPK3. Therefore, we investigated the effect of ferrostatin-1 and liproxstatin-1, two recently described inhibitors of ferroptosis (Dixon et al. 2012; Dong et al. 2015; Friedmann Angeli et al. 2014; Skouta et al. 2014; Yang et al. 2014). Ferrostatin-1 and liproxstatin-1 are able to quench radical species thereby preventing lipid peroxidation (Kabiraj et al. 2015; Skouta et al. 2014; Zilka et al. 2017). *t*-BuOOH-induced cell death was almost completely blocked by ferrostatin-1 or liproxstatin-1, both in NIH3T3 and in HaCaT cells (Fig. 5a, b) strongly indicating ferroptosis. In line with our conclusion, cell death was also inhibited by the lipid antioxidant α-tocopherol and the iron chelator deferoxamine (Fig. 5a) (Dixon et al. 2012). In addition, the cell morphology of *t*-BuOOH-treated NIH3T3 cells (Supplementary Fig. S6)

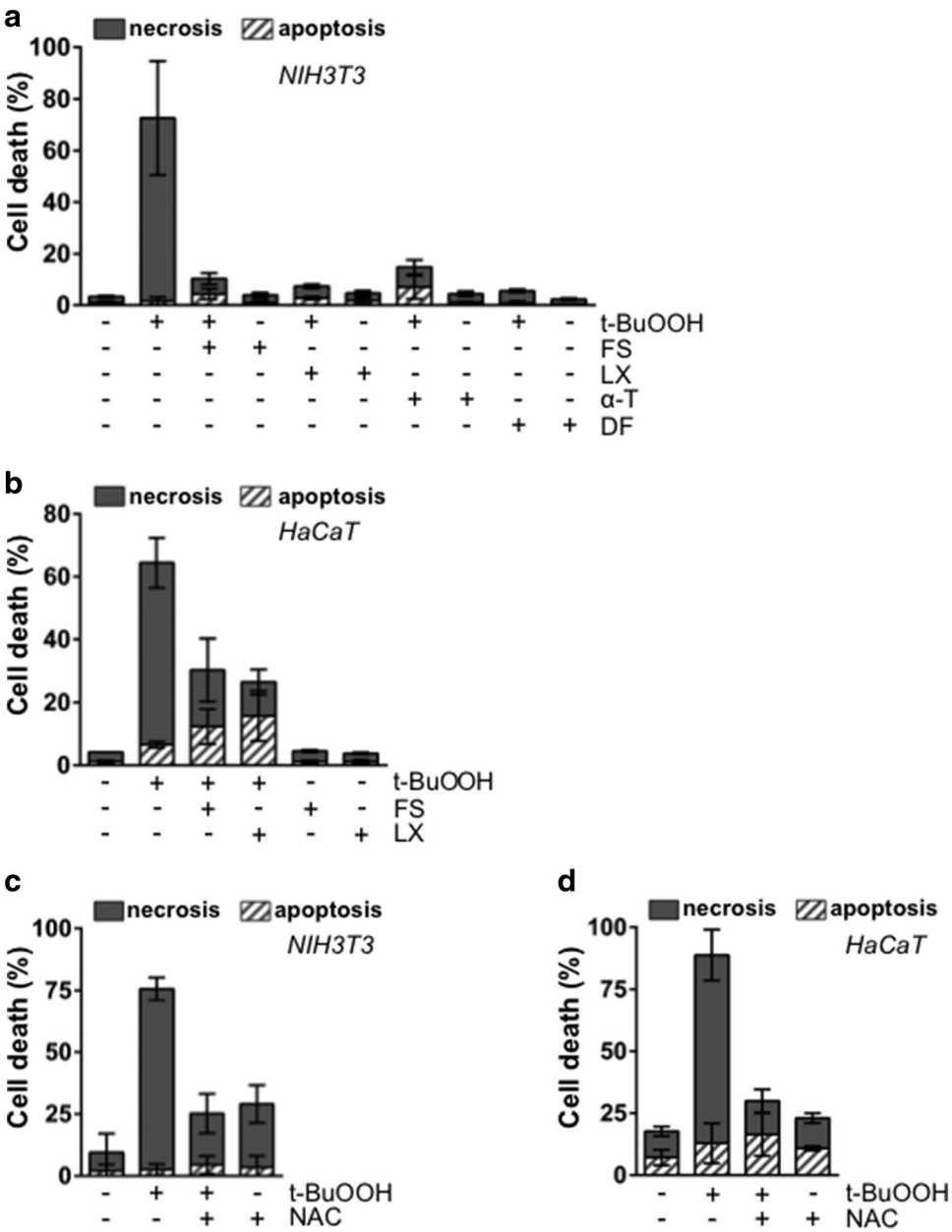

Fig. 5 *t*-BuOOH induces ferroptosis. **a–d** Determination of cell death. NIH3T3 (**a**, **c**) or HaCaT (**b**, **d**) cells were treated with *t*-BuOOH for 6 h in the absence or presence of the specific ferroptosis inhibitors ferrostatin-1 (FS, 1 µM) or liproxstatin-1 (LX, 1 µM) (**a**, **b**), α-tocopherol (α-T, 100 µM) or the iron chelator deferoxamine mesylate (DF, 100 µM) (**a**), or *N*-acetylcysteine (NAC, 1 mM) (**c**, **d**). Results are expressed as mean ± SD, $n = 3$–4 in duplicates. *t*-BuOOH-induced cell death was significantly ($p < 0.001$) inhibited by FS, LX, α-T, DF, or NAC

strongly resembled that of erastin-treated cells (Supplementary Fig. S6) (Dixon et al. 2012) or cells undergoing ferroptosis due to cystine deprivation (Gao et al. 2015). Our conclusion of a ferroptotic cell death event was supported by the fact that *t*-BuOOH-mediated cell death could be reversed by *N*-acetylcysteine (Fig. 5d, e). It has been shown that *t*-BuOOH reduces glutathione levels (Martin et al. 2001), which is known to enhance lipid peroxidation (Dixon et al. 2014). As shown for erastin treatment, *t*-BuOOH induced an increase in lipid peroxidation and cytosolic ROS which could be significantly reduced by ferrostatin-1 and liproxstatin-1, as assessed by flow cytometry using the lipid sensitive C11-Bodipy (Fig. 6a) and the cytosolic ROS probe H_2DCFDA (Fig. 6b). Hence, the data strongly indicate that *t*-BuOOH induces ferroptosis.

As shown above, *t*-BuOOH-triggered cell death is independent from p53. Recently, a role of p53 in ferroptosis has been described. p53 sensitizes cells against ferroptosis by inducing glutaminolysis (Gao et al. 2015), by inhibiting cystine import (Jiang et al. 2015a, b) or by inducing SAT1 (spermidine/spermine N^1-acetyltransferase-1) and thereby arachidonate 15-lipoxygenase (Alox15) (Ou et al. 2016). We, therefore, investigated whether $p53^{-/-}$ fibroblasts died by ferroptosis in response to *t*-BuOOH and also focused on earlier timepoints to discover a possible sensitization. Both ferrostatin-1 and liproxstatin-1 blocked

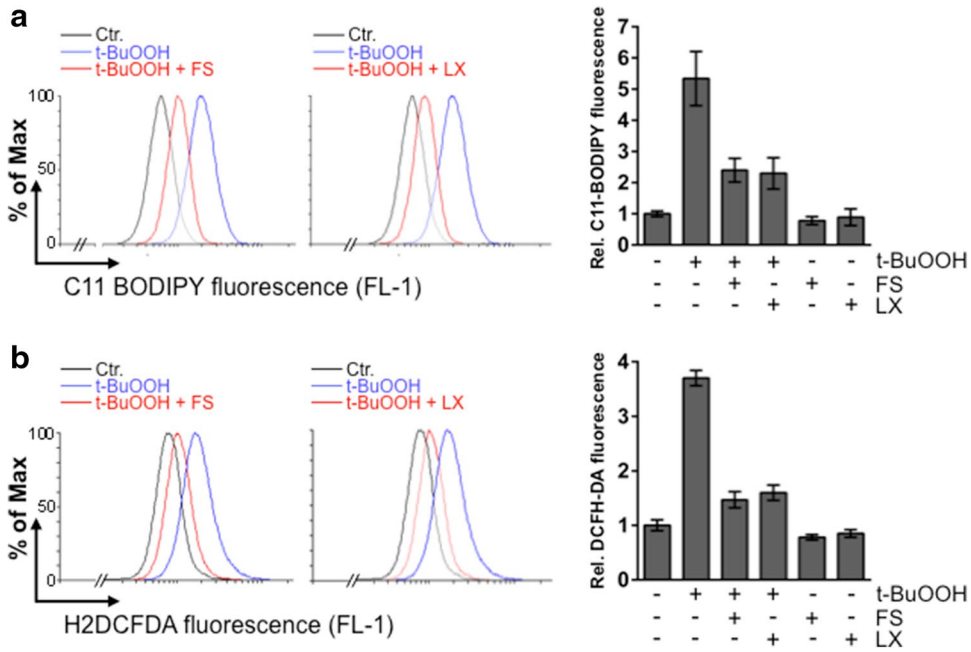

Fig. 6 *t*-BuOOH induces an increase in lipid peroxidation and cytosolic ROS. NIH3T3 cells were treated with *t*-BuOOH in the absence or the presence of FS or LX either for 3 h and lipid peroxidation was measured using the lipid peroxidation sensor Bodipy 581/591 C11 (**a**) or for 2 h and cytosolic ROS was measured using 2-7-dichlorodihydrofluorescein diacetate (H_2DCFDA) (**b**). (Left) Representative experiments. (Right) Results are expressed relative to controls (untreated = 1). Bars represent the mean ± SD, $n = 7–15$. *t*-BuOOH significantly ($p < 0.001$) induced an increase in lipid peroxidation and cytosolic ROS which was significantly ($p < 0.001$) reduced by FS or LX

t-BuOOH-mediated cell death in wt- and $p53^{-/-}$ fibroblasts suggesting ferroptosis as the main cell death pathway (Supplementary Fig. S7). However, $p53^{-/-}$ fibroblasts were slightly less sensitive to *t*-BuOOH after 6 h of *t*-BuOOH treatment compared to wt cells (but not at later timepoints, see Fig. 2a). We conclude that p53 slightly sensitizes mouse fibroblasts against ferroptosis, but that p53 is not required for *t*-BuOOH-triggered ferroptosis.

t-BuOOH-triggered ferroptosis is dependent on cardiolipin oxidation, but executed independently from collapse of MMP

Having identified ferroptosis as the main cell death pathway in response to *t*-BuOOH, we further investigated potential triggers of ferroptosis and a possible crosstalk with other lethal pathways. An interplay between DNA damage and mitochondria has not only been demonstrated in apoptosis, but also in regulated necrosis induced by ROS or alkylating agents (Andrabi et al. 2008; Fu et al. 2013). In contrast to the established and specific ferroptosis inducers erastin (Dixon et al. 2012) or RSL3 (Yang et al. 2014), *t*-BuOOH induces a plethora of cellular damages, such as collapse of MMP, DNA DSBs, or replication block (Avery 2011) and it was likely that these damages contribute to *t*-BuOOH-triggered ferroptosis. Indeed, *t*-BuOOH induced a time-dependent breakdown of the MMP as detected by a decrease in DiOC6 staining (Fig. 7a) as well as NAD^+ depletion (Supplementary Fig. S8). Neither ferrostatin-1 nor liproxstatin-1 blocked *t*-BuOOH-triggered loss of the MMP (Fig. 7a). Together with the observation that olaparib attenuated *t*-BuOOH-mediated decrease in NAD^+ (Supplementary Fig. S8), but did not diminish cell death, we conclude that neither loss of MMP nor NAD^+ depletion contributes to *t*-BuOOH-induced ferroptosis. Moreover, cell death and collapse of MMP could not be reversed by cyclosporine A (Supplementary Fig. S9), which prevents opening of the mitochondrial transition pore (Giorgio et al. 2010). This is in line with results obtained in erastin-induced ferroptosis (Dixon et al. 2012). However, dissipation of the MMP is a typical feature of ferroptosis (Yagoda et al. 2007), albeit the functional role of the mitochondria in ferroptosis is not entirely clear. Recent data indicate that oxidation of cardiolipins, which are concentrated in the inner mitochondrial membrane, is essential for ferroptosis (Ji et al. 2012; Krainz et al. 2016). To better understand the role of mitochondria in *t*-BuOOH-triggered ferroptosis, we analyzed two recently described inhibitors of cardiolipin oxidation, i.e., JP4-039 and the mitochondria-selective XJB-5-131 (Ji et al. 2012; Krainz et al. 2016; Wipf et al. 2005). XJB-5-131 almost completely, and JP4-039 strongly blocked *t*-BuOOH-induced cell death (Fig. 7b), indicating that oxidation of cardiolipins is crucial for *t*-BuOOH-mediated ferroptosis and that mitochondrial lipid signaling is likely to play a significant role in this pathway. However, loss of MMP could not be reversed by XJB-5-131 or JP4-039 (Supplementary Fig. S10). Our data show that mitochondria play a major role in the execution of *t*-BuOOH-triggered ferroptosis, but that breakdown of MMP is not involved.

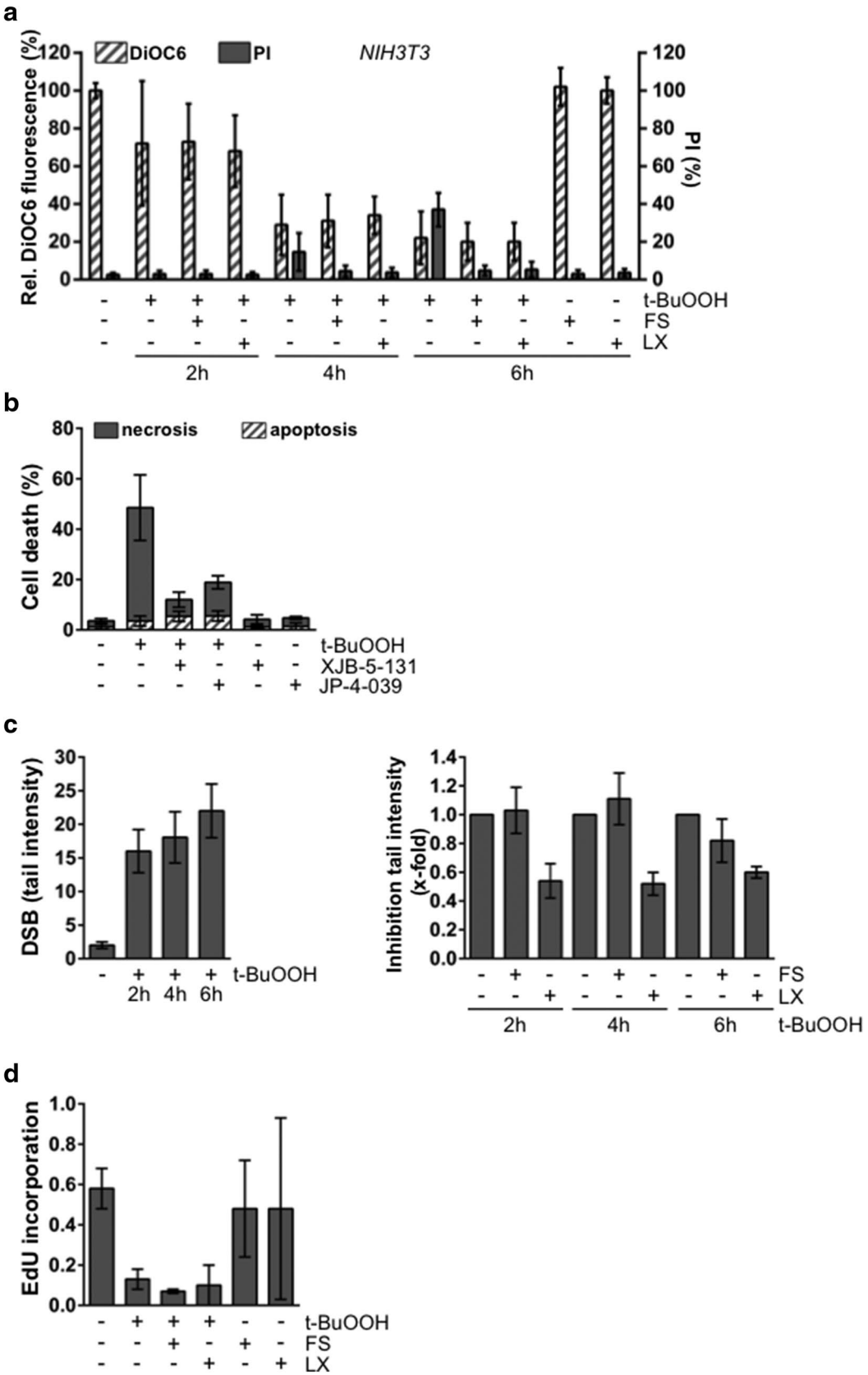
a
DiOC6
PI
NIH3T3
Rel. DiOC6 fluorescence (%)
PI (%)
t-BuOOH
FS
LX
2h
4h
6h
b
necrosis
apoptosis
Cell death (%)
t-BuOOH
XJB-5-131
JP-4-039
c
DSB (tail intensity)
t-BuOOH
2h 4h 6h
Inhibition tail intensity (x-fold)
FS
LX
2h
4h
6h
t-BuOOH
d
EdU incorporation
t-BuOOH
FS
LX

◂**Fig. 7** *t*-BuOOH-triggered ferroptosis is executed independently from dissipation of the MMP, is dependent on mitochondrial cardiolipin oxidation, and is independent from DNA damage. **a** Simultaneous DiOC6 and PI staining to determine mitochondrial and cellular viability. NIH3T3 cells were treated for the indicated time periods with *t*-BuOOH in the absence or the presence of FS or LX. Results are expressed as mean ± SD, $n = 4–5$. Loss of MMP was significant ($p < 0.001$) after 4 h of *t*-BuOOH treatment. FS or LX did not prevent loss of MMP, but significantly ($p < 0.001$) inhibited cell death. **b** Determination of cell death. NIH3T3 cells were treated for 6 h with *t*-BuOOH in the absence or the presence of XJB-5-131 (1 µM) or JP4-039 (10 µM). Results are expressed as mean ± SD, $n = 3–5$. XJB-5-131 and JP4-039 significantly ($p < 0.001$) blocked *t*-BuOOH-triggered cell death. **c** Neutral Comet assay to detect DNA DSBs. (Left) NIH3T3 cells were treated with *t*-BuOOH for the indicated time periods. Results are expressed as mean ± SD, $n = 10–11$. Induction of DSBs was significant ($p < 0.001$) at every indicated timepoint. (Right) NIH3T3 cells were treated with *t*-BuOOH in the absence or the presence of FS or LX. FS did not inhibit DSB formation and LX partially, but significantly (2, 4 h: $p < 0.01$; 6 h: $p < 0.05$) blocked *t*-BuOOH-mediated DSB formation ($n = 4–11$). **d** EdU staining. Proliferating NIH3T3 cells were treated for 2 h with *t*-BuOOH in the absence or the presence of FS or LX. Replication block was demonstrated by the reduction of EdU-positive S-phase cells. Results are expressed as mean ± SD, $n = 3$. *t*-BuOOH significantly ($p < 0.001$) inhibited replication

t-BuOOH-triggered ferroptosis is executed independently from DNA DSB formation or replication block

We finally investigated a potential crosstalk between DNA damage, especially DSBs and replication block, and the signaling of ferroptosis. DSBs are known to be highly toxic DNA lesions and their role in apoptosis has been extensively studied (Lips and Kaina 2001; Roos et al. 2016). Growing evidence suggests that DNA damage may also trigger necroptosis (Geserick et al. 2015; Koo et al. 2015). A role of DNA damage in ferroptosis has not been studied so far. Using neutral Comet assay, we detected a strong increase in DSB formation in response to *t*-BuOOH (Fig. 7c). DSB formation was not reversed by ferrostatin-1, and only partially attenuated by liproxstatin-1 (Fig. 7c). Finally, we focused on a potential crosstalk between ferroptosis and replication block. Replication block, for instance, induced by hydroxy urea, has been shown to induce apoptosis and to sensitize against radio- and chemotherapy (Kramer et al. 2008; Schrell et al. 1997; Seiwert et al. 2007; Stauber et al. 2012). *t*-BuOOH clearly induced a replication block (Fig. 7d). However, *t*-BuOOH-mediated replication block could not be prevented by ferrostatin-1 or liproxstatin-1 as assessed by the incorporation of EdU (Fig. 7d).

H_2O_2 does not induce ferroptosis

Importantly, cell death mediated by H_2O_2, used at an equitoxic concentration (300 µM), could not be attenuated by ferrostatin-1 or liproxstatin-1 (Fig. 8a) which is in line with previous observations (Dixon et al. 2014). It is noteworthy that Dixon and coworkers used much higher concentrations of *t*-BuOOH than we did. We found that (1) H_2O_2 induced significantly less lipid peroxidation (about twofold) than *t*-BuOOH (> 5-fold) and (2) H_2O_2-mediated lipid peroxidation was not altered by ferrostatin-1 nor liproxstatin-1 (Fig. 8b). Increasing the concentrations of H_2O_2 did not elevate, but rather diminished the amount of lipid peroxidation (Supplementary Fig. S11). However, we have not tested lower concentrations of H_2O_2. Our data suggest that the lipid peroxidation products caused by *t*-BuOOH differ not only quantitatively, but also qualitatively from those induced by H_2O_2 at least at the concentrations tested. Hence, our data demonstrate that *t*-BuOOH, but not H_2O_2, causes formation of specific lipid peroxidation products leading to ferroptosis.

Conclusions

Exploring the mechanisms of ferroptosis is of great importance. On one hand, it could help to identify new targets to treat ferroptosis occurring in pathological situations, such as acute kidney injury, myocardial infarction, liver necrosis, or neuronal degenerative diseases (Kers et al. 2016; Muller et al. 2017; Yang and Stockwell 2016). On the other hand, some tumor types seem to be sensitive towards ferroptosis-inducing compounds (Xie et al. 2016; Yang and Stockwell 2016), suggesting that ferroptosis is a promising approach to kill cancer cells which are, for instance, resistant to apoptosis.

Here, we present *t*-BuOOH as a novel inducer of ferroptosis. Remarkably, *t*-BuOOH-driven ferroptosis is executed independently from DNA damage or loss of MMP. To date, only a few activators of ferroptosis have been identified (Xie et al. 2016). It is generally assumed that downregulation of the GSH/GPX4 defense system leads to an increase in lipid peroxidation which causes ferroptosis. Lipid peroxidation in response to erastin or GPX4 inhibition is driven enzymatically by Alox15 (Friedmann Angeli et al. 2014; Yang et al. 2016). Although it is not clear how cell death is finally executed, oxidized polyunsaturated fatty acids (PUFAs), and/or thereof derived breakdown products, such as 4-hydroxynonenal, are supposed to be essential for ferroptosis (Magtanong et al. 2016). Very recently, it has been shown that ferroptosis is induced by peroxidation of ω-6 fatty acids, especially arachidonic acid and adrenic acid in phosphatidyl ethanolamine (Doll et al. 2017; Kagan et al. 2017; Yang et al. 2016). It is known that *t*-BuOOH nonenzymatically leads to formation of primary alkoxyl- (*t*-BO$^{\cdot}$) and secondary formed peroxyl radicals (*t*-BOO$^{\cdot}$) which abstract hydrogen from PUFAs, thereby

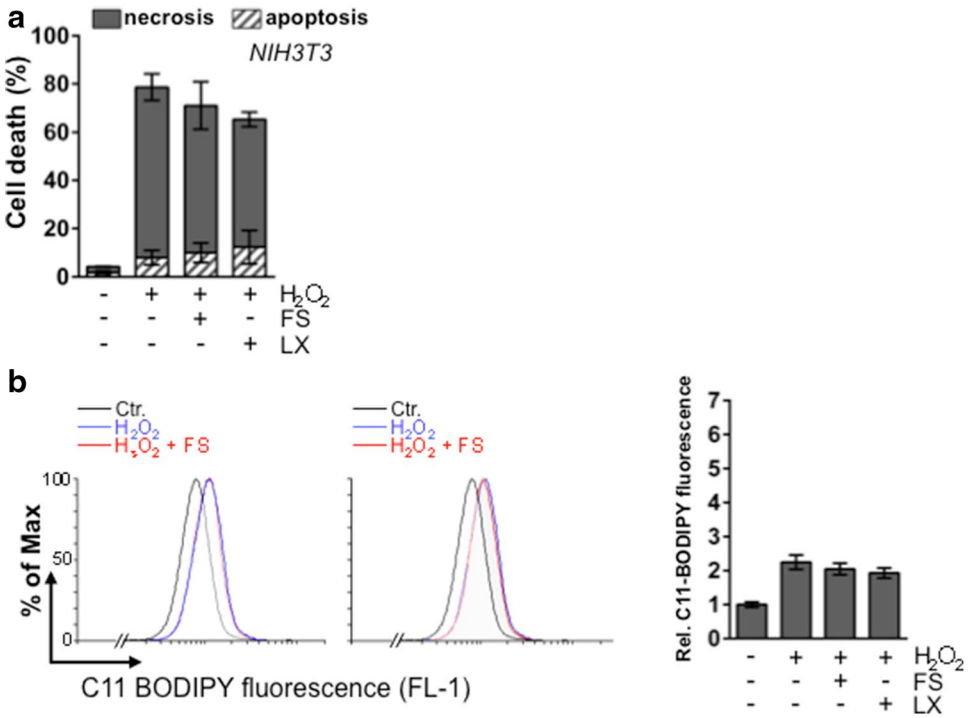

Fig. 8 H_2O_2 does not induce ferroptosis. **a** Determination of cell death. NIH3T3 cells were treated with H_2O_2 (300 µM) for 6 h in the presence of FS or LX. Results are expressed as mean ± SD, $n = 3$ in duplicates. **b** Detection of lipid peroxidation. NIH3T3 cells were treated with H_2O_2 (300 µM) for 3 h in the absence or the presence of FS or LX. (Left) representative experiment. (Right) bars representing the mean ± SD, $n = 3$ in duplicates

initiating lipid peroxidation (Barr and Mason 1995; Hix et al. 2000; Masaki et al. 1989). Lipid peroxidation is then propagated by a chain reaction for which transition metals, such as iron, are required (Cheng and Li 2007). Although the data need to be confirmed, first experiments suggest that *t*-BuOOH-mediated lipid peroxidation is indeed independent from Alox15. Whether *t*-BuOOH induces a similar lipid peroxidation pattern to erastin or RSL3 has yet to be analyzed. The involvement of other potential players in *t*-BuOOH-triggered ferroptosis, such as GPX4, NOX enzymes (Dixon et al. 2012), lysosomes (Torii et al. 2016), endoplasmatic reticulum stress (Dixon et al. 2014), or autophagy (Gao et al. 2016), also remains to be investigated.

t-BuOOH seems to be unique as a trigger for ferroptosis among commonly used chemical ROS inducers. Other ROS-producing agents, such as H_2O_2 or rotenone, do not cause ferroptosis (own work) (Dixon et al. 2012). We conclude that different ROS inducers may trigger different cell death pathways which might rely on the nature, the amount, the kinetics, and/or the subcellular localization of the ROS species formed. The reason why *t*-BuOOH leads to a specific, ferroptosis-inducing lipid peroxidation pattern remains to be resolved. However, understanding the difference between these compounds will help to better understand the regulation of ferroptosis.

Acknowledgements We thank Bernd Epe for fruitful discussions. We are indebted to Anna Frumkina for expert technical assistance. The technical support by Julia Altmaier, FACS, and Array Core Facility is gratefully acknowledged. The work was supported by the Stipendienstiftung Rheinland-Pfalz, Hoffmann-Klose-Stiftung, Johannes Gutenberg-University, and University Medical Center of the Johannes Gutenberg-University and is part of the Ph.D. thesis of CW and the MD theses of BL, CT, and ASS. SK acknowledges support from Dr. Werner Jackstädt-Stiftung and Fresenius Medical Care Germany.

Compliance with ethical standards

Conflict of interest The authors declare that they have no conflict of interest.

References

Alia M, Ramos S, Mateos R, Bravo L, Goya L (2005) Response of the antioxidant defense system to tert-butyl hydroperoxide and hydrogen peroxide in a human hepatoma cell line (HepG2). J Biochem Mol Toxicol 19(2):119–128. doi:10.1002/jbt.20061

Amoroso S, D'Alessio A, Sirabella R, Di Renzo G, Annunziato L (2002) Ca(2+)-independent caspase-3 but not Ca(2+)-dependent caspase-2 activation induced by oxidative stress leads to SH-SY5Y human neuroblastoma cell apoptosis. J Neurosci Res 68(4):454–462. doi:10.1002/jnr.10199

Andrabi SA, Dawson TM, Dawson VL (2008) Mitochondrial and nuclear cross talk in cell death: parthanatos. Ann N Y Acad Sci 1147:233–241. doi:10.1196/annals.1427.014

Avery SV (2011) Molecular targets of oxidative stress. Biochem J 434(2):201–210. doi:10.1042/BJ20101695

Ayala A, Munoz MF, Arguelles S (2014) Lipid peroxidation: production, metabolism, and signaling mechanisms of malondialdehyde and 4-hydroxy-2-nonenal. Oxid Med Cell Longev 2014:360438. doi:10.1155/2014/360438

Baines CP, Kaiser RA, Purcell NH et al (2005) Loss of cyclophilin D reveals a critical role for mitochondrial permeability transition in cell death. Nature 434(7033):658–662. doi:10.1038/nature03434

Baker MA, He SQ (1991) Elaboration of cellular DNA breaks by hydroperoxides. Free Radic Biol Med 11(6):563–572

Barr DP, Mason RP (1995) Mechanism of radical production from the reaction of cytochrome c with organic hydroperoxides. An ESR spin trapping investigation. J Biol Chem 270(21):12709–12716

Bennett BL, Sasaki DT, Murray BW et al (2001) SP600125, an anthrapyrazolone inhibitor of Jun N-terminal kinase. Proc Natl Acad Sci USA 98(24):13681–13686. doi:10.1073/pnas.251194298

Bergamini CM, Gambetti S, Dondi A, Cervellati C (2004) Oxygen, reactive oxygen species and tissue damage. Curr Pharm Des 10(14):1611–1626

Berger SB, Harris P, Nagilla R et al (2015) Characterization of GSK'963: a structurally distinct, potent and selective inhibitor of RIP1 kinase. Cell Death Discov 1:15009. doi:10.1038/cddiscovery.2015.9

Boukamp P, Petrussevska RT, Breitkreutz D, Hornung J, Markham A, Fusenig NE (1988) Normal keratinization in a spontaneously immortalized aneuploid human keratinocyte cell line. J Cell Biol 106(3):761–771

Cao JY, Dixon SJ (2016) Mechanisms of ferroptosis. Cell Mol Life Sci 73(11–12):2195–2209. doi:10.1007/s00018-016-2194-1

Cheng Z, Li Y (2007) What is responsible for the initiating chemistry of iron-mediated lipid peroxidation: an update. Chem Rev 107(3):748–766. doi:10.1021/cr040077w

Chiu LY, Ho FM, Shiah SG, Chang Y, Lin WW (2011) Oxidative stress initiates DNA damager MNNG-induced poly(ADP-ribose)polymerase-1-dependent parthanatos cell death. Biochem Pharmacol 81(3):459–470. doi:10.1016/j.bcp.2010.10.016

Coleman JB, Gilfor D, Farber JL (1989) Dissociation of the accumulation of single-strand breaks in DNA from the killing of cultured hepatocytes by an oxidative stress. Mol Pharmacol 36(1):193–200

Conrad M, Angeli JP, Vandenabeele P, Stockwell BR (2016) Regulated necrosis: disease relevance and therapeutic opportunities. Nat Rev Drug Discov 15(5):348–366. doi:10.1038/nrd.2015.6

Cuenda A, Rouse J, Doza YN et al (1995) SB 203580 is a specific inhibitor of a MAP kinase homologue which is stimulated by cellular stresses and interleukin-1. FEBS Lett 364(2):229–233

Degterev A, Huang Z, Boyce M et al (2005) Chemical inhibitor of nonapoptotic cell death with therapeutic potential for ischemic brain injury. Nat Chem Biol 1(2):112–119. doi:10.1038/nchembio711

Deng X, Xiao L, Lang W, Gao F, Ruvolo P, May WS Jr (2001) Novel role for JNK as a stress-activated Bcl2 kinase. J Biol Chem 276(26):23681–23688. doi:10.1074/jbc.M100279200

Dietrich C, Wallenfang K, Oesch F, Wieser R (1997) Differences in the mechanisms of growth control in contact-inhibited and serum-deprived human fibroblasts. Oncogene 15(22):2743–2747. doi:10.1038/sj.onc.1201439

Dixon SJ (2017) Ferroptosis: bug or feature? Immunol Rev 277(1):150–157. doi:10.1111/imr.12533

Dixon SJ, Lemberg KM, Lamprecht MR et al (2012) Ferroptosis: an iron-dependent form of nonapoptotic cell death. Cell 149(5):1060–1072. doi:10.1016/j.cell.2012.03.042

Dixon SJ, Patel DN, Welsch M et al (2014) Pharmacological inhibition of cystine-glutamate exchange induces endoplasmic reticulum stress and ferroptosis. Elife 3:e02523. doi:10.7554/eLife.02523

Doll S, Proneth B, Tyurina YY et al (2017) ACSL4 dictates ferroptosis sensitivity by shaping cellular lipid composition. Nat Chem Biol 13(1):91–98. doi:10.1038/nchembio.2239

Dondelinger Y, Declercq W, Montessuit S et al (2014) MLKL compromises plasma membrane integrity by binding to phosphatidylinositol phosphates. Cell Rep 7(4):971–981. doi:10.1016/j.celrep.2014.04.026

Dong T, Liao D, Liu X, Lei X (2015) Using small molecules to dissect non-apoptotic programmed cell death: necroptosis, ferroptosis, and pyroptosis. ChemBioChem 16(18):2557–2561. doi:10.1002/cbic.201500422

Eling N, Reuter L, Hazin J, Hamacher-Brady A, Brady NR (2015) Identification of artesunate as a specific activator of ferroptosis in pancreatic cancer cells. Oncoscience 2(5):517–532. doi:10.18632/oncoscience.160

Faust D, Nikolova T, Watjen W, Kaina B, Dietrich C (2017) The Brassica-derived phytochemical indolo[3,2-b]carbazole protects against oxidative DNA damage by aryl hydrocarbon receptor activation. Arch Toxicol 91(2):967–982. doi:10.1007/s00204-016-1672-4

Friedemann T, Otto B, Klatschke K et al (2014) Coptis chinensis Franch. exhibits neuroprotective properties against oxidative stress in human neuroblastoma cells. J Ethnopharmacol 155(1):607–615. doi:10.1016/j.jep.2014.06.004

Friedmann Angeli JP, Schneider M, Proneth B et al (2014) Inactivation of the ferroptosis regulator Gpx4 triggers acute renal failure in mice. Nat Cell Biol 16(12):1180–1191. doi:10.1038/ncb3064

Fu D, Jordan JJ, Samson LD (2013) Human ALKBH7 is required for alkylation and oxidation-induced programmed necrosis. Genes Dev 27(10):1089–1100. doi:10.1101/gad.215533.113

Fulda S (2014) Therapeutic exploitation of necroptosis for cancer therapy. Semin Cell Dev Biol 35:51–56. doi:10.1016/j.semcdb.2014.07.002

Gaballah M, Slisz M, Hutter-Lobo D (2012) Role of JNK-1 regulation in the protection of contact-inhibited fibroblasts from oxidative stress. Mol Cell Biochem 359(1–2):105–113. doi:10.1007/s11010-011-1004-1

Galluzzi L, Vitale I, Abrams JM et al (2012) Molecular definitions of cell death subroutines: recommendations of the Nomenclature Committee on Cell Death 2012. Cell Death Differ 19(1):107–120. doi:10.1038/cdd.2011.96

Galluzzi L, Kepp O, Krautwald S, Kroemer G, Linkermann A (2014) Molecular mechanisms of regulated necrosis. Semin Cell Dev Biol 35:24–32. doi:10.1016/j.semcdb.2014.02.006

Gao M, Monian P, Quadri N, Ramasamy R, Jiang X (2015) Glutaminolysis and transferrin regulate ferroptosis. Mol Cell 59(2):298–308. doi:10.1016/j.molcel.2015.06.011

Gao M, Monian P, Pan Q, Zhang W, Xiang J, Jiang X (2016) Ferroptosis is an autophagic cell death process. Cell Res 26(9):1021–1032. doi:10.1038/cr.2016.95

Garcia-Cohen EC, Marin J, Diez-Picazo LD, Baena AB, Salaices M, Rodriguez-Martinez MA (2000) Oxidative stress induced by tert-butyl hydroperoxide causes vasoconstriction in the aorta from hypertensive and aged rats: role of cyclooxygenase-2 isoform. J Pharmacol Exp Ther 293(1):75–81

Geserick P, Wang J, Schilling R et al (2015) Absence of RIPK3 predicts necroptosis resistance in malignant melanoma. Cell Death Dis 6:e1884. doi:10.1038/cddis.2015.240

Giorgio V, Soriano ME, Basso E et al (2010) Cyclophilin D in mitochondrial pathophysiology. Biochem Biophys Acta 1797(6–7):1113–1118. doi:10.1016/j.bbabio.2009.12.006

Gong YN, Guy C, Olauson H et al (2017) ESCRT-III acts downstream of MLKL to regulate necroptotic cell death and its consequences. Cell 169(2):286–300.e16. doi:10.1016/j.cell.2017.03.020

Ha HC, Snyder SH (1999) Poly(ADP-ribose) polymerase is a mediator of necrotic cell death by ATP depletion. Proc Natl Acad Sci USA 96(24):13978–13982

Halestrap AP (2009) What is the mitochondrial permeability transition pore? J Mol Cell Cardiol 46(6):821–831. doi:10.1016/j.yjmcc.2009.02.021

Hampton MB, Orrenius S (1997) Dual regulation of caspase activity by hydrogen peroxide: implications for apoptosis. FEBS Lett 414(3):552–556

Hix S, Kadiiska MB, Mason RP, Augusto O (2000) In vivo metabolism of tert-butyl hydroperoxide to methyl radicals. EPR spin-trapping and DNA methylation studies. Chem Res Toxicol 13(10):1056–1064

Ji J, Kline AE, Amoscato A et al (2012) Lipidomics identifies cardiolipin oxidation as a mitochondrial target for redox therapy of brain injury. Nat Neurosci 15(10):1407–1413. doi:10.1038/nn.3195

Jiang L, Hickman JH, Wang SJ, Gu W (2015a) Dynamic roles of p53-mediated metabolic activities in ROS-induced stress responses. Cell Cycle (Georgetown, Tex) 14(18):2881–2885. doi:10.1080/15384101.2015.1068479

Jiang L, Kon N, Li T et al (2015b) Ferroptosis as a p53-mediated activity during tumour suppression. Nature 520(7545):57–62. doi:10.1038/nature14344

Kabiraj P, Valenzuela CA, Marin JE et al (2015) The neuroprotective role of ferrostatin-1 under rotenone-induced oxidative stress in dopaminergic neuroblastoma cells. Protein J 34(5):349–358. doi:10.1007/s10930-015-9629-7

Kagan VE, Mao G, Qu F et al (2017) Oxidized arachidonic and adrenic PEs navigate cells to ferroptosis. Nat Chem Biol 13(1):81–90. doi:10.1038/nchembio.2238

Kanupriya Prasad D, Sai Ram M, Sawhney RC, Ilavazhagan G, Banerjee PK (2007) Mechanism of tert-butylhydroperoxide induced cytotoxicity in U-937 macrophages by alteration of mitochondrial function and generation of ROS. Toxicol In Vitro 21(5):846–854. doi:10.1016/j.tiv.2007.02.007

Kers J, Leemans JC, Linkermann A (2016) An overview of pathways of regulated necrosis in acute kidney injury. Semin Nephrol 36(3):139–152. doi:10.1016/j.semnephrol.2016.03.002

Kim OS, Kim YS, Jang DS, Yoo NH, Kim JS (2009) Cytoprotection against hydrogen peroxide-induced cell death in cultured mouse mesangial cells by erigeroflavanone, a novel compound from the flowers of Erigeron annuus. Chem Biol Interact 180(3):414–420

Koo GB, Morgan MJ, Lee DG et al (2015) Methylation-dependent loss of RIP3 expression in cancer represses programmed necrosis in response to chemotherapeutics. Cell Res 25(6):707–725. doi:10.1038/cr.2015.56

Krainz T, Gaschler MM, Lim C, Sacher JR, Stockwell BR, Wipf P (2016) A mitochondrial-targeted nitroxide is a potent inhibitor of ferroptosis. ACS Cent Sci 2(9):653–659. doi:10.1021/acscentsci.6b00199

Kramer OH, Knauer SK, Zimmermann D, Stauber RH, Heinzel T (2008) Histone deacetylase inhibitors and hydroxyurea modulate the cell cycle and cooperatively induce apoptosis. Oncogene 27(6):732–740. doi:10.1038/sj.onc.1210677

Kreuzaler P, Watson CJ (2012) Killing a cancer: what are the alternatives? Nat Rev Cancer 12(6):411–424. doi:10.1038/nrc3264

Lackinger D, Eichhorn U, Kaina B (2001) Effect of ultraviolet light, methyl methanesulfonate and ionizing radiation on the genotoxic response and apoptosis of mouse fibroblasts lacking c-Fos, p53 or both. Mutagenesis 16(3):233–241

Laemmli UK (1970) Cleavage of structural proteins during the assembly of the head of bacteriophage T4. Nature 227(5259):680–685

Lehman TA, Modali R, Boukamp P et al (1993) p53 mutations in human immortalized epithelial cell lines. Carcinogenesis 14(5):833–839

Leist M, Single B, Castoldi AF, Kuhnle S, Nicotera P (1997) Intracellular adenosine triphosphate (ATP) concentration: a switch in the decision between apoptosis and necrosis. J Exp Med 185(8):1481–1486

Lemasters JJ, Nieminen AL (1997) Mitochondrial oxygen radical formation during reductive and oxidative stress to intact hepatocytes. Biosci Rep 17(3):281–291

Linden A, Gulden M, Martin HJ, Maser E, Seibert H (2008) Peroxide-induced cell death and lipid peroxidation in C6 glioma cells. Toxicol In Vitro 22(5):1371–1376. doi:10.1016/j.tiv.2008.02.003

Linkermann A, Green DR (2014) Necroptosis. N Engl J Med 370(5):455–465. doi:10.1056/NEJMra1310050

Linkermann A, Brasen JH, Darding M et al (2013) Two independent pathways of regulated necrosis mediate ischemia-reperfusion injury. Proc Natl Acad Sci USA 110(29):12024–12029. doi:10.1073/pnas.1305538110

Linkermann A, Skouta R, Himmerkus N et al (2014a) Synchronized renal tubular cell death involves ferroptosis. Proc Natl Acad Sci USA 111(47):16836–16841. doi:10.1073/pnas.1415518111

Linkermann A, Stockwell BR, Krautwald S, Anders HJ (2014b) Regulated cell death and inflammation: an auto-amplification loop causes organ failure. Nat Rev Immunol 14(11):759–767. doi:10.1038/nri3743

Lips J, Kaina B (2001) DNA double-strand breaks trigger apoptosis in p53-deficient fibroblasts. Carcinogenesis 22(4):579–585

Magtanong L, Ko PJ, Dixon SJ (2016) Emerging roles for lipids in non-apoptotic cell death. Cell Death Differ 23(7):1099–1109. doi:10.1038/cdd.2016.25

Mandal P, Berger SB, Pillay S et al (2014) RIP3 induces apoptosis independent of pronecrotic kinase activity. Mol Cell 56(4):481–495. doi:10.1016/j.molcel.2014.10.021

Martin C, Martinez R, Navarro R, Ruiz-Sanz JI, Lacort M, Ruiz-Larrea MB (2001) tert-Butyl hydroperoxide-induced lipid signaling in hepatocytes: involvement of glutathione and free radicals. Biochem Pharmacol 62(6):705–712

Martin MA, Serrano AB, Ramos S, Pulido MI, Bravo L, Goya L (2010) Cocoa flavonoids up-regulate antioxidant enzyme activity via the ERK1/2 pathway to protect against oxidative stress-induced apoptosis in HepG2 cells. J Nutr Biochem 21(3):196–205. doi:10.1016/j.jnutbio.2008.10.009

Masaki N, Kyle ME, Farber JL (1989) tert-Butyl hydroperoxide kills cultured hepatocytes by peroxidizing membrane lipids. Arch Biochem Biophys 269(2):390–399

Menear KA, Adcock C, Boulter R et al (2008) 4-[3-(4-cyclopropanecarbonylpiperazine-1-carbonyl)-4-fluorobenzyl]-2H-phthalazin- 1-one: a novel bioavailable inhibitor of poly(ADP-ribose) polymerase-1. J Med Chem 51(20):6581–6591. doi:10.1021/jm8001263

Mohammad RM, Muqbil I, Lowe L et al (2015) Broad targeting of resistance to apoptosis in cancer. Semin Cancer Biol 35(Suppl):S78–S103. doi:10.1016/j.semcancer.2015.03.001

Montero J, Dutta C, van Bodegom D, Weinstock D, Letai A (2013) p53 regulates a non-apoptotic death induced by ROS. Cell Death Differ 20(11):1465–1474. doi:10.1038/cdd.2013.52

Muller T, Dewitz C, Schmitz J et al (2017) Necroptosis and ferroptosis are alternative cell death pathways that operate in acute kidney failure. Cell Mol Life Sci. doi:10.1007/s00018-017-2547-4

Nicotera P, Melino G (2004) Regulation of the apoptosis-necrosis switch. Oncogene 23(16):2757–2765. doi:10.1038/sj.onc.1207559

Ou Y, Wang SJ, Li D, Chu B, Gu W (2016) Activation of SAT1 engages polyamine metabolism with p53-mediated ferroptotic responses. Proc Natl Acad Sci USA 113(44):E6806–E6812. doi:10.1073/pnas.1607152113

Pereira L, Igea A, Canovas B, Dolado I, Nebreda AR (2013) Inhibition of p38 MAPK sensitizes tumour cells to cisplatin-induced apoptosis mediated by reactive oxygen species and JNK. EMBO Mol Med 5(11):1759–1774. doi:10.1002/emmm.201302732

Redza-Dutordoir M, Averill-Bates DA (2016) Activation of apoptosis signalling pathways by reactive oxygen species. Biochem Biophys Acta 12(1863):2977–2992. doi:10.1016/j.bbamcr.2016.09.012

Roos WP, Thomas AD, Kaina B (2016) DNA damage and the balance between survival and death in cancer biology. Nat Rev Cancer 16(1):20–33. doi:10.1038/nrc.2015.2

Sabapathy K, Jochum W, Hochedlinger K, Chang L, Karin M, Wagner EF (1999) Defective neural tube morphogenesis and altered apoptosis in the absence of both JNK1 and JNK2. Mech Dev 89(1–2):115–124

Saito Y, Nishio K, Ogawa Y et al (2006) Turning point in apoptosis/necrosis induced by hydrogen peroxide. Free Radical Res 40(6):619–630. doi:10.1080/10715760600632552

Schrell UM, Rittig MG, Anders M et al (1997) Hydroxyurea for treatment of unresectable and recurrent meningiomas. I. Inhibition of primary human meningioma cells in culture and in meningioma transplants by induction of the apoptotic pathway. J Neurosurg 86(5):845–852. doi:10.3171/jns.1997.86.5.0845

Sedelnikova OA, Redon CE, Dickey JS, Nakamura AJ, Georgakilas AG, Bonner WM (2010) Role of oxidatively induced DNA lesions in human pathogenesis. Mutat Res 704(1–3):152–159. doi:10.1016/j.mrrev.2009.12.005

Seiwert TY, Salama JK, Vokes EE (2007) The chemoradiation paradigm in head and neck cancer. Nat Clin Pract Oncol 4(3):156–171. doi:10.1038/ncponc0750

Shen HM, Lin Y, Choksi S et al (2004) Essential roles of receptor-interacting protein and TRAF2 in oxidative stress-induced cell death. Mol Cell Biol 24(13):5914–5922. doi:10.1128/MCB.24.13.5914-5922.2004

Skouta R, Dixon SJ, Wang J et al (2014) Ferrostatins inhibit oxidative lipid damage and cell death in diverse disease models. J Am Chem Soc 136(12):4551–4556. doi:10.1021/ja411006a

Smith PK, Krohn RI, Hermanson GT et al (1985) Measurement of protein using bicinchoninic acid. Anal Biochem 150(1):76–85

Sosa V, Moline T, Somoza R, Paciucci R, Kondoh H, LLeonart ME (2013) Oxidative stress and cancer: an overview. Ageing Res Rev 12(1):376–390. doi:10.1016/j.arr.2012.10.004

Stauber RH, Knauer SK, Habtemichael N et al (2012) A combination of a ribonucleotide reductase inhibitor and histone deacetylase inhibitors downregulates EGFR and triggers BIM-dependent apoptosis in head and neck cancer. Oncotarget 3(1):31–43. doi:10.18632/oncotarget.430

Temkin V, Huang Q, Liu H, Osada H, Pope RM (2006) Inhibition of ADP/ATP exchange in receptor-interacting protein-mediated necrosis. Mol Cell Biol 26(6):2215–2225. doi:10.1128/MCB.26.6.2215-2225.2006

Tonnus W, Linkermann A (2017) The in vivo evidence for regulated necrosis. Immunol Rev 277(1):128–149. doi:10.1111/imr.12551

Torii S, Shintoku R, Kubota C et al (2016) An essential role for functional lysosomes in ferroptosis of cancer cells. Biochem J 473(6):769–777. doi:10.1042/BJ20150658

Vanden Berghe T, Vanlangenakker N, Parthoens E et al (2010) Necroptosis, necrosis and secondary necrosis converge on similar cellular disintegration features. Cell Death Differ 17(6):922–930. doi:10.1038/cdd.2009.184

Vanden Berghe T, Linkermann A, Jouan-Lanhouet S, Walczak H, Vandenabeele P (2014) Regulated necrosis: the expanding network of non-apoptotic cell death pathways. Nat Rev Mol Cell Biol 15(2):135–147. doi:10.1038/nrm3737

Vandenabeele P, Grootjans S, Callewaert N, Takahashi N (2013) Necrostatin-1 blocks both RIPK1 and IDO: consequences for the study of cell death in experimental disease models. Cell Death Differ 20(2):185–187. doi:10.1038/cdd.2012.151

Vanlangenakker N, Vanden Berghe T, Vandenabeele P (2012) Many stimuli pull the necrotic trigger, an overview. Cell Death Differ 19(1):75–86. doi:10.1038/cdd.2011.164

Vaseva AV, Marchenko ND, Ji K, Tsirka SE, Holzmann S, Moll UM (2012) p53 opens the mitochondrial permeability transition pore to trigger necrosis. Cell 149(7):1536–1548. doi:10.1016/j.cell.2012.05.014

Vroegop SM, Decker DE, Buxser SE (1995) Localization of damage induced by reactive oxygen species in cultured cells. Free Radic Biol Med 18(2):141–151

Wang Y (2008) Bulky DNA lesions induced by reactive oxygen species. Chem Res Toxicol 21(2):276–281. doi:10.1021/tx700411g

Wang Y, Dawson VL, Dawson TM (2009) Poly(ADP-ribose) signals to mitochondrial AIF: a key event in parthanatos. Exp Neurol 218(2):193–202. doi:10.1016/j.expneurol.2009.03.020

Wang Z, Jiang H, Chen S, Du F, Wang X (2012) The mitochondrial phosphatase PGAM5 functions at the convergence point of multiple necrotic death pathways. Cell 148(1–2):228–243. doi:10.1016/j.cell.2011.11.030

Watanabe T, Sekine S, Naguro I, Sekine Y, Ichijo H (2015) Apoptosis signal-regulating kinase 1 (ASK1)-p38 pathway-dependent cytoplasmic translocation of the orphan nuclear receptor NR4A2 is required for oxidative stress-induced necrosis. J Biol Chem 290(17):10791–10803. doi:10.1074/jbc.M114.623280

Wipf P, Xiao J, Jiang J et al (2005) Mitochondrial targeting of selective electron scavengers: synthesis and biological analysis of hemigramicidin-TEMPO conjugates. J Am Chem Soc 127(36):12460–12461. doi:10.1021/ja053679l

Xia Y, Ongusaha P, Lee SW, Liou YC (2009) Loss of Wip1 sensitizes cells to stress- and DNA damage-induced apoptosis. J Biol Chem 284(26):17428–17437. doi:10.1074/jbc.M109.007823

Xie Y, Hou W, Song X et al (2016) Ferroptosis: process and function. Cell Death Differ 23(3):369–379. doi:10.1038/cdd.2015.158

Xu H, Luo P, Zhao Y et al (2013) Iduna protects HT22 cells from hydrogen peroxide-induced oxidative stress through interfering poly(ADP-ribose) polymerase-1-induced cell death (parthanatos). Cell Signal 25(4):1018–1026. doi:10.1016/j.cellsig.2013.01.006

Yagoda N, von Rechenberg M, Zaganjor E et al (2007) RAS-RAF-MEK-dependent oxidative cell death involving voltage-dependent anion channels. Nature 447(7146):864–868. doi:10.1038/nature05859

Yang WS, Stockwell BR (2016) Ferroptosis: death by lipid peroxidation. Trends Cell Biol 26(3):165–176. doi:10.1016/j.tcb.2015.10.014

Yang WS, SriRamaratnam R, Welsch ME et al (2014) Regulation of ferroptotic cancer cell death by GPX4. Cell 156(1–2):317–331. doi:10.1016/j.cell.2013.12.010

Yang WS, Kim KJ, Gaschler MM, Patel M, Shchepinov MS, Stockwell BR (2016) Peroxidation of polyunsaturated fatty acids by lipoxygenases drives ferroptosis. Proc Natl Acad Sci USA 113(34):E4966–E4975. doi:10.1073/pnas.1603244113

Zhang S, Lin Y, Kim YS, Hande MP, Liu ZG, Shen HM (2007) c-Jun N-terminal kinase mediates hydrogen peroxide-induced cell death via sustained poly(ADP-ribose) polymerase-1 activation. Cell Death Differ 14(5):1001–1010. doi:10.1038/sj.cdd.4402088

Zhang DW, Zheng M, Zhao J et al (2011) Multiple death pathways in TNF-treated fibroblasts: RIP3- and RIP1-dependent and independent routes. Cell Res 21(2):368–371. doi:10.1038/cr.2011.3

Zilka O, Shah R, Li B et al (2017) On the mechanism of cytoprotection by ferrostatin-1 and liproxstatin-1 and the role of lipid peroxidation in ferroptotic cell death. ACS Cent Sci 3(3):232–243. doi:10.1021/acscentsci.7b00028